Journal of Materials Chemistry C

PAPER

View Article Online
View Journal | View Issue

Cite this: J. Mater. Chem. C, 2014, 2, 3278

Influence of fluorine substituents on the film dielectric constant and open-circuit voltage in organic photovoltaics†

Pinyi Yang,[a] Mingjian Yuan,[a] David F. Zeigler,[b] Scott E. Watkins,[c] Jason A. Lee[b] and Christine K. Luscombe*[a]

Received 22nd October 2013
Accepted 16th December 2013

DOI: 10.1039/c3tc32087a

www.rsc.org/MaterialsC

Conjugated polymers with fluorine substituents on their backbone have exhibited improved performance over their un-fluorinated analogues by lowering the polymer HOMO level, thereby increasing the open-circuit voltage (V_{OC}). To further investigate how fluorine substituents improve device performance, three polymers with the same donor and acceptor co-monomers, but differing by the number of fluorine atoms on the acceptor unit, were synthesized. Although the HOMO levels of the mono-(**P1F**) and di-fluorinated (**P2F**) polymers are essentially the same, an increase in V_{OC} was still observed in the OPV device incorporating **P2F**. This implies that correlating the V_{OC} to the donor polymer HOMO level is inadequate to fully explain the improvement in V_{OC}. By calculating the charge transfer exciton binding energy from the measured film dielectric constant, it was found that the increase in V_{OC} in going from **P1F** to **P2F** matches the decrease in charge transfer exciton binding energy.

Introduction

Bulk-heterojunction (BHJ) organic photovoltaics (OPVs) using π-conjugated polymers as the light-harvesting electron donor have shown promise as a low-cost and low-carbon renewable energy source. To achieve OPVs with high efficiencies, efforts have been devoted to develop π-conjugated polymers with enhanced optical and electrical properties to improve the short-circuit current density (J_{SC}), open-circuit voltage (V_{OC}), fill factor (FF), and ultimately, the power conversion efficiency (PCE).[1–5] Recently, π-conjugated polymers with fluorine atoms as substituents on the polymer backbone have been shown to greatly enhance the performance of several high performing polymers.[6–9] Since they are strongly electron-withdrawing, fluorine atoms lower the highest occupied molecular orbital (HOMO) level of a given π-conjugated polymer when compared to its non-fluorinated counterpart.[4,6,10] Because the V_{OC} of OPV devices is primarily determined by the energy difference between the HOMO of the electron donor and lowest unoccupied molecular orbital (LUMO) of the electron acceptor, an enhanced V_{OC} is expected in conjugated polymers with fluorine substituents. This effect has been proposed as the main factor for the performance improvement observed in OPVs containing fluorinated polymers.[6,10–12] Besides lowering the HOMO of conjugated polymers, fluorine substituents have also been reported to play a role in enhancing J_{SC}, V_{OC} and FF of OPVs by: (1) reducing bimolecular recombination and (2) increasing the charge dipole moment thereby suppressing geminate recombination.[10,13–15]

To obtain a better understanding of the working principle of fluorine substituents on the donor polymer on the V_{OC} of OPVs, and to separate out the effect of how lowering the HOMO of the donor polymers affects the V_{OC}, we synthesized the following three polymers, PBnDT-DPNT **P0F**, PBnDT-DPfNT **P1F** and PBnDT-DPffNT **P2F** (Fig. 1), which were designed to have approximately the same HOMO levels while having a differing number of fluorine groups. Both material properties and their optimized OPV devices were characterized. Despite the minimal difference between the HOMO levels of **P1F** and **P2F**, **P2F** showed an enhanced V_{OC} in OPVs. This enabled the investigation of the fluorine substituents' impact on the V_{OC} beyond that of shifting the donor polymer HOMO level. A quantitative relationship between the fluorine substitution and V_{OC} was built by using a more precise equation including the charge transfer exciton binding energy.

Experimental procedure

General measurement and characterization

All chemicals were purchased from Aldrich or VWR and used as received unless otherwise specified. Molecules **1**,[16] **5**,[16] **9**[17] and

[a]Department of Materials Science and Engineering and Molecular Engineering and Sciences Institute, University of Washington, Box 352120, Seattle, WA 98195-2120, USA. E-mail: luscombe@uw.edu

[b]Department of Chemistry, University of Washington, Box 351700, Seattle, WA 98195-1700, USA

[c]Ian Wark Laboratory, CSIRO Molecular and Health Technologies, Clayton South, Victoria 3169, Australia

† Electronic supplementary information (ESI) available: Calculated frontier orbitals, PESA, and capacitance measurements. See DOI: 10.1039/c3tc32087a

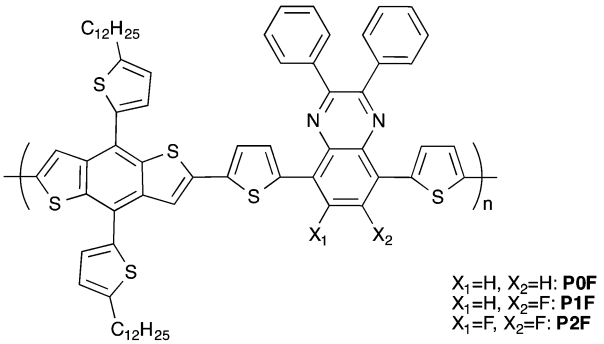

Fig. 1 Molecular structures of (a) PBnDT-DPNT **P0F**, (b) PBnDT-DPfNT **P1F** and (c) PBnDT-DPffNT **P2F**.

10[18] were synthesized according to previous literature procedures. ^{1}H NMR and ^{13}C NMR spectra were collected on a Bruker Avance DPS-300 spectrometer. Mass spectrometry was performed using a Hewlett-Packard 5971A gas chromatograph and Bruker Bi flex III MALDI-TOF (both positive and negative ion reflector mode). The molecular weights of the polymers were measured using a Viscotek TDA 305 with a polystyrene standard (room temperature, THF as eluent). The absorption spectra were measured using a Perkins-Elmer Lambda-9 spectrophotometer.

5,8-Dibromo-6-fluoro-2,3-diphenylquinoxaline 2. A mixture of 2,5-dibromo-4-fluoro-5,6-benzenediamine **1** (0.85 g, 3.0 mmol) and benzil (0.63 g, 3 mmol) in 30 mL of acetic acid was refluxed overnight. After cooling to room temperature, the solution was poured into water and extracted with dichloromethane. The combined organic layers were dried over Na_2SO_4. After removal of the solvent under reduced pressure, the crude product was purified by column chromatography and then recrystallized to give a light yellow solid (1.1 g, 83%). ^{1}H NMR ($CDCl_3$, ppm): 7.94 (s, 1H), 7.70–7.66 (m, 4H), 7.44–7.35 (m, 6H). ^{13}C NMR ($CDCl_3$, ppm): 158.72, 141.37, 140.25, 136.70, 133.25, 130.67, 129.43, 127.54. MS (ESI): ($[M^+H]^+$, $C_{20}H_{11}Br_2FN_2$), calcd, 455.9; found: 460.9.

6-Fluoro-2,3-diphenyl-5,8-di(thiophene-2-yl)quinoxaline 3. Compound **2** (0.9 g, 2 mmol), 2-(tributylstannyl)thiophene (1.87 g, 5 mmol), and $Pd(PPh_3)_4$ (46 mg, 0.04 mmol) were added to a 50 mL two-neck flask and dissolved in degassed toluene (30 mL). The mixture was heated to 90 °C under nitrogen overnight. The resulting solution was extracted with ethyl acetate and washed with brine. The combined organic layers were dried over Na_2SO_4. After removal of the solvent under reduced pressure, the residue was purified by column chromatography on silica gel (hexane/DCM, v/v, 5 : 1) to give compound **3** as orange crystals (659 mg, 71%). ^{1}H NMR ($CDCl_3$, ppm): 7.61 (s, 1H), 7.63–7.57 (m, 6H), 7.46–7.32 (m, 6H), 7.15 (m, 2H), 7.02 (d, 2H). ^{13}C NMR ($CDCl_3$, ppm): 163.21, 160.23, 154.17, 145.27, 142.35, 133.23, 130.06, 129.09, 127.98, 125.31. MALDI-TOF: ($C_{28}H_{17}FN_2S_2$), calcd, 464.1; found: 463.0.

5,8-Bis(5-bromothiophen-2-yl)-6-fluoro-2,3-diphenylquinoxaline 4. Compound **3** (464 mg, 1 mmol) was dissolved in chloroform (15 mL), and then NBS (360 mg, 2 mmol) was added to the solution at 0 °C. The resulting mixture was stirred at room temperature for another 2 h. The solution was then poured into 2 M Na_2CO_3 and extracted with chloroform. The combined organic layers were dried over anhydrous Na_2SO_4, the solvent was removed under reduced pressure, and the residue was purified by silica gel chromatography with hexane as the eluent to get compound **4** as an orange solid (528 mg, 81%). ^{1}H NMR ($CDCl_3$, ppm): 7.70 (s, 1H), 7.68–7.69 (m, 6H), 7.47–7.31 (m, 4H), 7.07 (m, 2H), 6.93 (d, 2H). ^{13}C NMR ($CDCl_3$, ppm): 165.72, 163.31, 156.07, 148.90, 144.6, 137.43, 136.27, 133.51, 128.12, 125.03. MALDI-TOF: ($C_{28}H_{15}Br_2FN_2S_2$), calcd, 619.9; found: 619.0 (Scheme 1).

5,8-Dibromo-6,7-difluoro-2,3-diphenylquinoxaline 6. The mixture of 2,5-dibromo-3,4-difluoro-5,6-benzenediamine **5** (0.6 g, 2.0 mmol) and benzil (0.42 g, 2 mmol) in 20 mL of acetic acid was refluxed overnight. After cooling to room temperature, the solution was poured into water and extracted with dichloromethane. After removing solvent, the crude product was purified by column chromatography, followed by re-crystallization to give a light yellow solid (0.74 g, 77%). ^{1}H NMR ($CDCl_3$, ppm): 7.70–7.66 (m, 4H), 7.44–7.35 (m, 6H). ^{13}C NMR ($CDCl_3$, ppm): 152.34, 144.37, 141.87, 139.15, 136.76, 135.47, 130.28, 125.73. MALDI-TOF: ($C_{20}H_{10}Br_2F_2N_2$), calcd, 473.9; found: 472.6.

6,7-Difluoro-2,3-diphenyl-5,8-di(thiophene-2-yl)quinoxaline 7. Compound **6** (0.9 g, 2 mmol), 2-(tributylstannyl)thiophene (1.87 g, 5 mmol), and $Pd(PPh_3)_4$ (46 mg, 0.04 mmol) were added to a 50 mL two-neck flask and dissolved in degassed toluene (30 mL). The mixture was heated to 90 °C under nitrogen overnight. The resulting solution was extracted with ethyl acetate and washed with brine. The combined organic layers were dried over Na_2SO_4. After removal of the solvent under reduced pressure, the residue was purified by column chromatography on silica gel (hexane/DCM, v/v, 5 : 1) to give compound **7** as a red solid (659 mg, 71%). ^{1}H NMR ($CDCl_3$, ppm): 7.66–7.61 (m, 6H), 7.42–7.33 (m, 6H). 7.21 (m, 2H), 7.13 (d, 2H). ^{13}C NMR ($CDCl_3$,

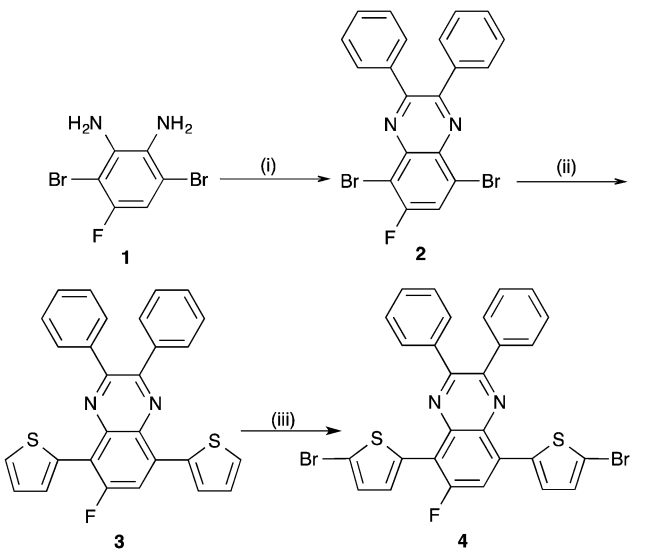

Scheme 1 Synthetic route for monomer **4**; (i) benzil, AcOH, reflux; (ii) 2-(tributylstannyl)thiophene, $Pd(PPh_3)_4$, toluene, 90 °C; (iii) NBS, $CHCl_3$.

ppm): 166.67, 163.42, 158.03, 146.74, 144.11, 135.47, 132.52, 130.13, 125.02, 121.63. MALDI-TOF: ($C_{28}H_{16}F_2N_2S_2$), calcd, 482.1; found: 481.0.

5,8-Bis(5-bromothiophen-2-yl)-6-fluoro-2,3-diphenylquinoxaline 8. Compound 7 (482 mg, 1 mmol) was dissolved in chloroform (15 mL), and then NBS (360 mg, 2 mmol) was added into the solution at 0 °C. The resulting mixture was stirred at room temperature for another 2 h. Then the solution was poured into 2 M Na_2CO_3 and extracted with chloroform. The combined organic layers were dried over anhydrous Na_2SO_4, the solvent was removed under reduced pressure, and the residue was purified by silica gel chromatograph with hexane as the eluent to get compound **8** as a red solid (427 mg, 67%). ^{1}H NMR ($CDCl_3$, ppm): 7.73–7.70 (m, 6H), 7.51–7.43 (m, 4H). 7.17 (m, 2H), 7.06 (d, 2H). ^{13}C NMR ($CDCl_3$, ppm): 162.07, 167.13, 154.76, 150.11, 141.37, 136.12, 135.97, 131.27, 127.83, 123.21. MALDI-TOF: ($C_{28}H_{14}Br_2F_2N_2S_2$), calcd, 637.9; found: 636.6 (Scheme 2).

General procedure for the polymerization

All the polymers were prepared by a similar procedure. To a Schlenk flask was introduced compound **10** (753.5 mg, 0.5 mmol), corresponding acceptor monomer **4**, **8**, or **9** (0.5 mmol), and anhydrous chlorobenzene (4 mL). The solution was flushed with nitrogen for 10 min, and then a catalytic amount of tris(dibenzylideneacetone) dipalladium(0) (8.6 mg, 3 mol%) and tri(*o*-tolyl)phosphine (22.9 mg, 15 mol%) was added into the solution. After the resulting flask was degassed thrice *via* a freeze–pump–thaw cycle, the mixture was stirred at 100 °C for 48 h. Then, the reaction was cooled to room temperature and added into methanol dropwise. The precipitate was collected by filtration and washed by Soxhlet extraction with methanol, acetone, hexane, and chloroform. The chloroform fraction was then concentrated and precipitated into methanol. The solid was filtered and dried under vacuum for 1 day.

Polymer PBDT-DTQU (**P0F**): red solid. Yield 83%. ^{1}H NMR ($CDCl_3$, ppm): 7.77 (br, 2H), 7.38–7.14 (m, 20H), 2.60 (br, 4H), 1.65–1.50 (m, 28H), 1.34–1.25 (m, 12H), 0.95–0.80 (m, 6H) M_n = 32.9 kg mol^{-1}, PDI = 2.70.

Polymer PBDT-DTFQU (**P1F**): red solid. Yield 78%. ^{1}H NMR ($CDCl_3$, ppm): 7.77 (br, 2H), 7.42–7.16 (m, 19H), 2.60 (br, 4H), 1.70–1.50 (m, 28H), 1.34–1.25 (m, 12H), 0.99–0.75 (m, 6H) M_n = 27.9 kg mol^{-1}, PDI = 3.20.

Polymer PBDT-DTDFQU (**P2F**): red solid. Yield 91%. ^{1}H NMR ($CDCl_3$, ppm): 7.77 (br, 2H), 7.45–7.15 (m, 18H), 2.59 (br, 4H), 1.64–1.51 (m, 28H), 1.41–1.25 (m, 12H), 1.00–0.88 (m, 6H) M_n = 33.4 kg mol^{-1}, PDI = 3.04 (Scheme 3).

Polymer films for cyclic voltammetry (CV) characterization were prepared by spin coat 4 mg mL^{-1} polymer solution in chlorobenzene onto a clean ITO substrate. Cyclic voltammetry was conducted in acetonitrile with 0.1 M of tetrabutylammonium hexafluorophosphate using a scan rate of 100 mV s^{-1}. ITO, Ag/AgCl, and Pt mesh were used as the working electrode, reference electrode, and counter electrode respectively. Films for photoelectron spectroscopy in air (PESA) and UV-vis were coated using the same conditions mentioned above but on glass substrates. PESA measurements were recorded with a Riken Keiki AC-2 PESA spectrometer with a power setting of 5 nW and a power number of 0.5. A Varian Cary 5000 UV-Vis-NIR spectrometer was used for UV-vis measurements.

Fabrication and characterization of BHJ devices

ITO/glass substrates were ultrasonically cleaned sequentially in detergent, water, acetone and isopropyl alcohol. The substrates were covered by a 30 nm layer of PEDOT:PSS by spin coating. After annealing in air at 140 °C for 10 min, the samples were cooled to room temperature. Polymers were dissolved in chlorobenzene (CB) at a concentration of 4 mg mL^{-1} and $PC_{61}BM$ was added to reach the optimized ratio (1 : 3). The solutions were then heated at 90 °C and stirred overnight. Prior to deposition, the solutions were filtered through a 0.2 μm filter and the substrates were transferred into a glovebox. The

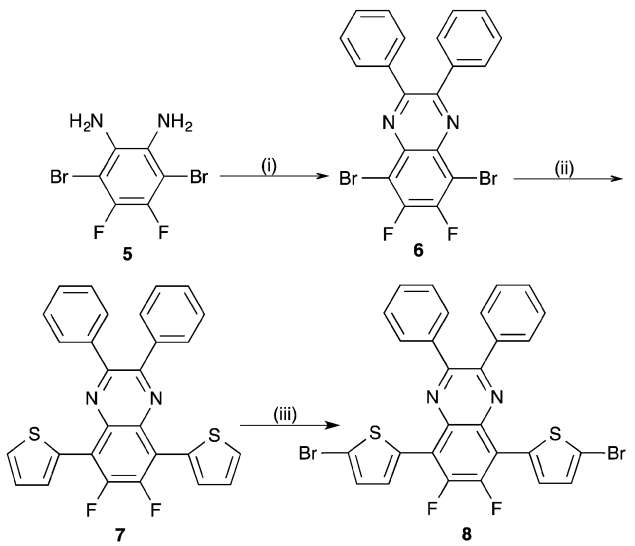

Scheme 2 Synthetic route for monomer **8**; (i) benzil, AcOH, reflux; (ii) 2-(tributylstannyl)thiophene, $Pd(PPh_3)_4$, toluene, 90 °C; (iii) NBS, $CHCl_3$.

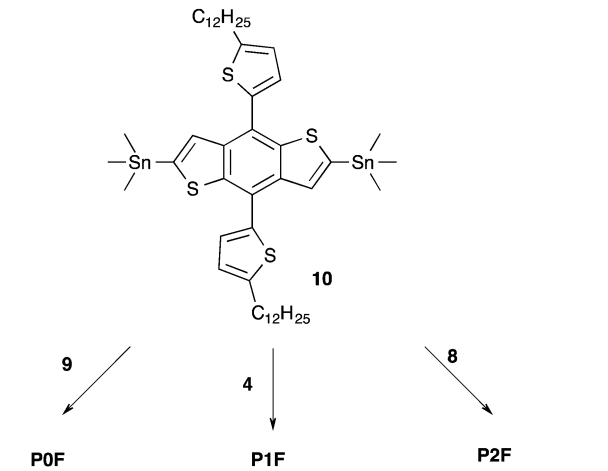

Scheme 3 Synthetic route for **P0F**, **P1F** and **P2F**; $Pd_2(dba)_3$, P(*o*-tolyl)$_3$, chlorobenzene, 100 °C.

photoactive layer was then spin-coated at different speeds to get a thickness about 100 nm. The aluminum cathode (100 nm thick) was thermally evaporated through a shadow mask under high vacuum about 4.0×10^{-7} torr. Devices were then tested using a Keithley 2400 source measurement unit, and an Oriel Xenon lamp (450 W) coupled with an AM1.5 filter was used as the light source. The light intensity was calibrated with a calibrated standard silicon solar cell with a KG5 filter which is traced to the National Renewable Energy Laboratory and a light intensity of 100 mW cm^{-2} was used in all the measurements in this study. Devices parameters were obtained by taking the average of 15 devices for each sample. Films for capacitance measurements were prepared on SiO_2 (300 nm)/Si substrate using the same procedure used for the fabrication OPV devices. The capacitance of each film was recorded with Agilent HP 4278A by applying a small voltage perturbation (20 mV rms) and sweeping frequencies from 1 MHz down to 20 Hz.

Result and discussion

Prior to their synthesis, density functional theory (DFT) quantum mechanical calculations at the B3LYP/6-31G level were performed to estimate the HOMO and LUMO energy levels of the polymers.[19,20] To minimize computing time, dimers of **P0F**, **P1F** and **P2F** were used and methyl groups replaced the alkyl chains for the simulation. The calculated HOMO and LUMO of the optimized structures are summarized in Fig. S1.† The calculated HOMO energy levels are −4.76 eV, −4.78 eV and −4.80 eV for **P0F**, **P1F** and **P2F** respectively (Table 1), which made them potentially good candidates to probe the origin of V_{OC} improvement upon fluorinating the acceptor unit. After polymer synthesis, the HOMO levels and band gaps of **P0F**, **P1F** and **P2F** films were measured using UV-vis spectrometry (Fig. 2(a)), CV (Fig. 2(b)), and PESA (Fig. S2†). The characterization results are summarized in Table 1.

The UV-vis of all three polymer thin films are shown in Fig. 2(a). Each of them shows an absorption band between 400 and 500 nm, and a second band between 500 and 700 nm. The first band can be attributed to the π–π* transition, while the band with lower energy is due to the intramolecular charge transfer (ICT) between the electron-rich and electron-deficient monomers.[19] Moreover, from the absorption edge of the thin films, it can be seen that their optical band gaps ($E_{g,opt}$) are nearly identical with values around 1.80 eV (Table 1). The small differences in the absorption spectra after fluorine substitution were previously reported in PBnDT-FTAZ and PTB4 as well,[6,21]

Table 1 Band gap and HOMO levels by different characterization methods of **P0F**, **P1F** and **P2F**

	Gaussian E_{HOMO} (eV)	$E_{g,opt}$ (eV)	E_{HOMO}[a] (eV)	E_{LUMO}[b] (eV)
P0F	−4.76	1.80	−4.98	−3.18
P1F	−4.78	1.80	−5.07	−3.27
P2F	−4.80	1.81	−5.08	−3.27

[a] Calculated based on $E_{HOMO} = -(4.8 - E_{1/2,Fc/Fc^+} + E_{ox,onset})$ eV. [b] Estimated from $E_{HOMO} = E_{LUMO} - E_{g,opt}$.

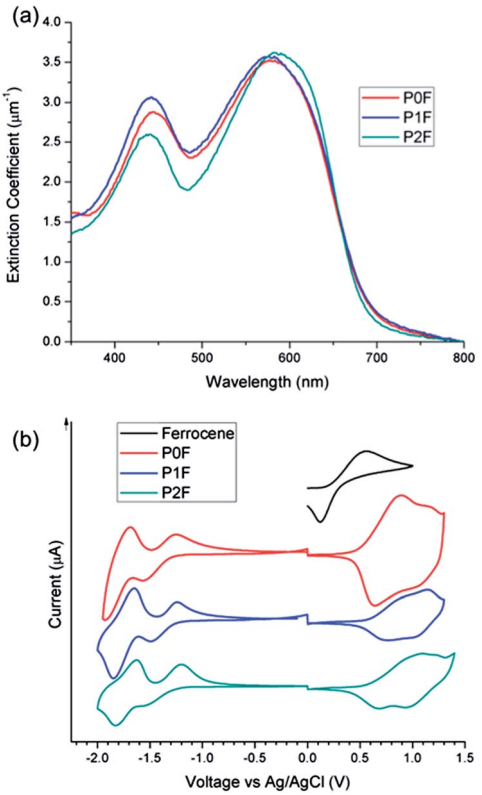

Fig. 2 (a) UV-vis spectra and (b) cyclic voltammograms of **P0F**, **P1F** and **P2F** films.

although in PCPDT-DFBT, the addition of fluorine atoms were found to cause a blue shift in the absorption spectrum.[21]

CV was employed to determine the HOMO energy levels (Fig. 2(b)). The HOMO energy levels were calculated from the onset oxidation potential *versus* Ag/AgCl using the equation $E_{HOMO} = -(4.8 - E_{1/2,Fc/Fc^+} + E_{ox,onset})$ eV. Stable and reversible oxidation behaviour was observed for all three polymers, revealing their p-type semiconductor nature. The HOMO energy levels of **P0F**, **P1F** and **P2F** were found to be −4.98 eV, −5.07 eV and −5.08 eV, respectively (Table 1) using CV. Although the HOMO energy level differences between **P0F** and the other two polymers are larger than the estimated values obtained using DFT, the HOMO energy levels of **P1F** and **P2F** are essentially the same. To further confirm the HOMO levels, films of all three polymers were characterized by PESA (Fig. S2†). The same 0.01 eV difference between **P1F** and **P2F** HOMO levels was still observed. The energy levels of all three polymers are summarized in Fig. 3. The $PC_{61}BM$ energy levels were previously reported and obtained using CV.[22,23] To be consistent with the $PC_{61}BM$ energy levels, we will be using HOMO levels obtained using CV for the rest of the discussion.

Optimized OPVs were fabricated by spin-coating polymer and [6,6]-phenyl-C61-butyric acid methyl ester (PCBM) blend solutions (1 : 3 ratio) in chlorobenzene onto indium tin oxide coated glass (ITO) with a pre-coated PEDOT:PSS layer. After drying in a nitrogen atmosphere overnight, the active layer thicknesses of photovoltaic devices were approximately 100 nm. Fig. 4(a) shows the *J*–*V* characteristics of OPVs

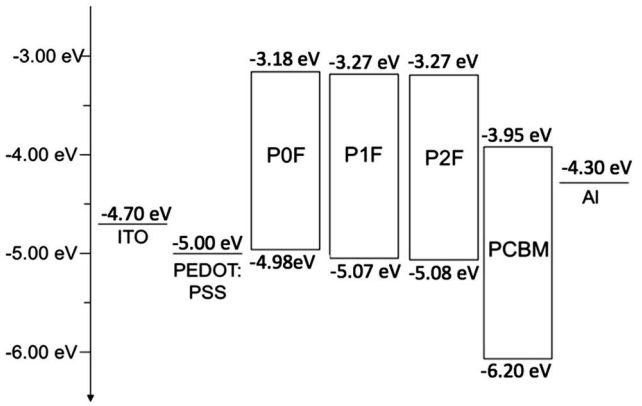

Fig. 3 Energy level diagram of **P0F**, **P1F** and **P2F** using data derived from CV and UV-vis spectra.

containing the three polymers. The device parameters are summarized in Table 2. All the device parameters increase upon addition of a fluorine atom on the polymer backbone. In most previously reported systems, the PCE enhancement of polymers with fluorine substituents was mainly due to either an increase in V_{OC}[10–12] or an increase in J_{SC} and FF.[24,25] However, in our case, all three parameters increased with each subsequent fluorine atom addition. The J_{SC} increased from 6.37 mA cm^{-2} in **P0F** to 6.52 mA cm^{-2} in **P1F** and to 6.84 mA cm^{-2} in **P2F**. Although the absorption of all three polymers is similar between 500 nm and 700 nm (Fig. 2(b)), the EQE (Fig. 4(b)) of the **P2F** device is the highest, while **P0F** and **P1F** devices show almost identical EQEs in that region. Dark current curves were also obtained. The excellent fit to the modified Schockley equation confirms the validity of our measured V_{OC} (Fig. S3 and Table S1†). Table S1† also lists the ideality factor, n, and the shunt resistance, R_{sh}, for all three devices. The similarity between the numbers shows that the extent of recombination is similar in all three devices.

The change in V_{OC} is surprising considering that all three polymers had similar HOMO levels. The V_{OC} of the devices increased from 0.832 V in **P0F** to 0.872 V in **P1F** and to 0.914 V in **P2F**. It increased by approximately the same amount (~0.04 V) with each additional fluorine substitution. If the V_{OC} is only related to energy difference between the LUMO of acceptor and the HOMO of donor,[26,27] the change in V_{OC} that we observe cannot be explained because they have nearly identical HOMO levels.

In order to further reveal the influence of fluorine substituents, a more precise relationship between the V_{OC} and energy levels of the active layer materials by using the concept of a charge transfer (CT) state is needed:[28–30]

$$V_{OC} = \frac{E^{A}_{LUMO} - E^{D}_{HOMO} - E^{CTE}_{B}}{q} - C \quad (1)$$

where E^{A}_{LUMO} is the LUMO energy level of acceptor, E^{D}_{HOMO} is the HOMO energy level of donor, E^{CTE}_{B} is the binding energy of charge transfer exciton (CTE), q is the elemental electron charge and C is a constant only related to illumination and

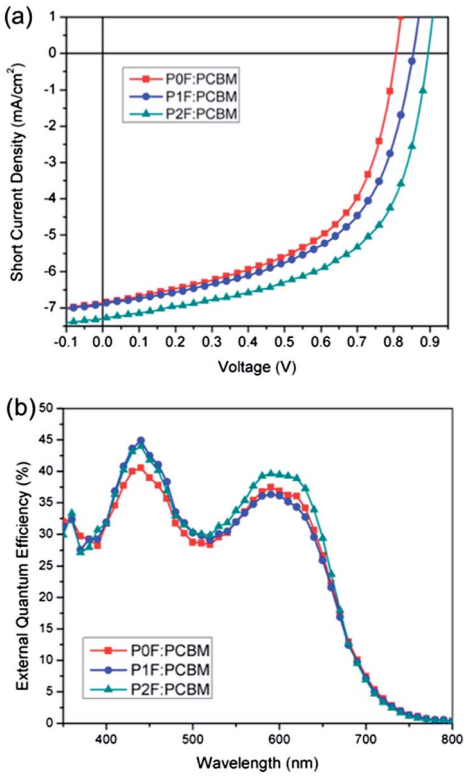

Fig. 4 (a) J–V characteristics of ITO/PEDOT:PSS/polymer: $PC_{61}BM$/Ca/Al under illumination of AM 1.5, 100 mW cm^{-2}. (b) EQE characteristics of the same devices.

temperature, which can be mainly attributed to voltage losses at the interface.[30] The CTEs can be thought of as being the precursor to the free carriers where a binding energy (E^{CTE}_{B}) must be overcome to form the free carriers. Moreover, the E^{CTE}_{B} can be estimated by:[31]

$$E^{CTE}_{B} = \frac{q^2}{4\pi\varepsilon_0\varepsilon_r r} \quad (2)$$

where ε_0 is the vacuum dielectric constant, ε_r is the relative average dielectric constant of the active layer and r is the radius of average initial CTE after charge transfer.[31]

The relative dielectric constants of **P0F**, **P1F** and **P2F** pure and blends films were calculated from the capacitance of each film on 300 nm SiO_2 layer (Fig. S4†). The E^{CTE}_{B} for each polymer was then estimated using the calculated relative dielectric constants and using $r = 1.5$ nm which is common in OPVs[29,30,32] although this value is expected to vary to a certain extent for each polymer. The E^{CTE}_{B} values and V_{OC} of all devices are summarized in Table 3. It can be seen that after adding the second fluorine, the relative dielectric constant of the blend film increased by 1 unit compared to a 0.2 increase by adding the first fluorine. As a result, the E^{CTE}_{B} in **P2F**:PCBM blend film has the lowest value of 0.18 eV, while the E^{CTE}_{B} for both **P0F**:PCBM and **P1F**:PCBM films are over 0.2 eV with values of 0.23 eV and 0.22 eV, respectively. According to eqn (1), as the E^{CTE}_{B} decreases by 0.04 eV from **P1F** to **P2F**, the V_{OC} of their devices should increase by 0.04 V, which is very close to the difference in

Table 2 Device parameters of optimized photovoltaic devices[a]

	$E^{A}_{LUMO} - E^{D}_{HOMO}$ (eV)	V_{OC} (V)	J_{SC} (mA cm^{-2})	FF	PCE (%)
P0F:PCBM	1.13	0.832 (0.003)	6.37 (0.05)	54% (1%)	2.9 (0.1)
P1F:PCBM	1.22	0.872 (0.003)	6.52 (0.07)	55% (1%)	3.1 (0.1)
P2F:PCBM	1.23	0.914 (0.002)	6.84 (0.03)	59% (1%)	3.7 (0.1)

[a] The device parameters reported are averages obtained from 15 devices. The number in parenthesis corresponds to the standard deviation of the measurements.

Table 3 Relative dielectric constant and estimated E^{CTE}_{B} of P0F, P1F and P2F pure and blends films

	Pure (ε_r)	Blend (ε_r)	E^{CTE}_{B} (eV)	Measured V_{OC} (V)	Calculated V_{OC} (V)
P0F	6.6	4.2	0.23	0.832	0.772[b]
P1F	7.2	4.4	0.22	0.872	0.872[a]
P2F	7.9	5.4	0.18	0.914	0.922[b]
Δ(**P0F** ⇒ **P1F**)	0.6	0.2	0.01	0.040	0.10
Δ(**P1F** ⇒ **P2F**)	0.7	1	0.04	0.042	0.05

[a] In order to calculate C, the measured V_{OC} value for **P1F**:PCBM was used. [b] In obtaining the calculated V_{OC} values, a constant C value was assumed.

experimental values (0.042 V). Moreover, because a lower E^{CTE}_{B} facilitates free carrier generation, the lower E^{CTE}_{B} also explains the higher EQE values between 500 nm and 700 nm in **P2F**:PCBM devices. Changes in E^{CTE}_{B} obtained from measuring bulk film properties and $E^{A}_{LUMO} - E^{D}_{HOMO}$ alone are insufficient to explain the V_{OC} difference observed between the **P0F** and **P1F** based devices. In this case, the change in V_{OC} may be a result of the change in local dipole moment that is observed when a fluorine atom is introduced.[13]

Conclusions

In summary, three conjugated polymers with 0, 1 and 2 fluorine substituents on the polymer backbone were synthesized. The HOMO levels of **P2F** and **P1F** were found to be nearly identical, and an enhancement V_{OC} was still observed in their PVs. By further investigating the V_{OC} change with a model involving the CTE binding energy, it was revealed that in addition to increasing V_{OC} by decreasing the HOMO levels of polymers, fluorine substituents are also able to affect the V_{OC} of OPVs by lowering the CTE binding energy.

Acknowledgements

This work was supported by a Research Corporation for Science Advancement Scialog award, NSF SOLAR Award DMR 1035196, and NSF EFRI-SEED Award 1038165.

Notes and references

1 F. Padinger, R. S. Rittberger and N. S. Sariciftci, *Adv. Funct. Mater.*, 2003, **13**, 85–88.
2 H. Hoppe and N. S. Sariciftci, *J. Mater. Chem.*, 2006, **16**, 45.
3 H. Hoppe, M. Niggemann, C. Winder, J. Kraut, R. Hiesgen, A. Hinsch, D. Meissner and N. S. Sariciftci, *Adv. Funct. Mater.*, 2004, **14**, 1005–1011.
4 H.-Y. Chen, J. Hou, S. Zhang, Y. Liang, G. Yang, Y. Yang, L. Yu, Y. Wu and G. Li, *Nat. Photonics*, 2009, **3**, 649–653.
5 Z. Li, J. Lu, S.-C. Tse, J. Zhou, X. Du, Y. Tao and J. Ding, *J. Mater. Chem.*, 2011, **21**, 3226.
6 S. C. Price, A. C. Stuart, L. Yang, H. Zhou and W. You, *J. Am. Chem. Soc.*, 2011, **133**, 4625–4631.
7 Y. Liang, Z. Xu, J. Xia, S.-T. Tsai, Y. Wu, G. Li, C. Ray and L. Yu, *Adv. Mater.*, 2010, **22**, E135–E138.
8 H. Zhou, L. Yang, A. C. Stuart, S. C. Price, S. Liu and W. You, *Angew. Chem., Int. Ed.*, 2011, **50**, 2995–2998.
9 Y. Li, J. Zou, H.-L. Yip, C.-Z. Li, Y. Zhang, C.-C. Chueh, J. Intemann, Y. Xu, P.-W. Liang, Y. Chen and A. K.-Y. Jen, *Macromolecules*, 2013, **46**, 5497–5503.
10 A. C. Stuart, J. R. Tumbleston, H. Zhou, W. Li, S. Liu, H. Ade and W. You, *J. Am. Chem. Soc.*, 2013, **135**, 1806–1815.
11 P. Heremans, D. Cheyns and B. P. Rand, *Acc. Chem. Res.*, 2009, **42**, 1740–1747.
12 S. Günes, H. Neugebauer and N. S. Sariciftci, *Chem. Rev.*, 2007, **107**, 1324–1338.
13 B. Carsten, J. M. Szarko, H. J. Son, W. Wang, L. Lu, F. He, B. S. Rolczynski, S. J. Lou, L. X. Chen and L. Yu, *J. Am. Chem. Soc.*, 2011, **133**, 20468–20475.
14 L. Yang, J. R. Tumbleston, H. Zhou, H. Ade and W. You, *Energy Environ. Sci.*, 2013, **6**, 316.
15 S. Albrecht, S. Janietz, W. Schindler, J. Frisch, J. Kurpiers, J. Kniepert, S. Inal, P. Pingel, K. Fostiropoulos, N. Koch and D. Neher, *J. Am. Chem. Soc.*, 2012, **134**, 14932–14944.
16 Y. Zhang, S.-C. Chien, K.-S. Chen, H.-L. Yip, Y. Sun, J. A. Davies, F.-C. Chen and A. K.-Y. Jen, *Chem. Commun.*, 2011, **47**, 11026–11028.
17 Y. Zhang, J. Zou, H.-L. Yip, K.-S. Chen, D. F. Zeigler, Y. Sun and A. K.-Y. Jen, *Chem. Mater.*, 2011, **23**, 2289–2291.
18 L. Huo, S. Zhang, X. Guo, F. Xu, Y. Li and J. Hou, *Angew. Chem., Int. Ed.*, 2011, **50**, 9697–9702.
19 M. Yuan, P. Yang, M. M. Durban and C. K. Luscombe, *Macromolecules*, 2012, **45**, 5934–5940.
20 T. M. McCormick, C. R. Bridges, E. I. Carrera, P. M. DiCarmine, G. L. Gibson, J. Hollinger, L. M. Kozycz and D. S. Seferos, *Macromolecules*, 2013, **46**, 3879–3886.
21 J. You, L. Dou, K. Yoshimura, T. Kato, K. Ohya, T. Moriarty, K. Emery, C.-C. Chen, J. Gao, G. Li and Y. Yang, *Nat. Commun.*, 2013, **4**, 1446.

22 S. H. Yoo, J. M. Kum and S. O. Cho, *Nanoscale Res. Lett.*, 2011, **6**, 545.
23 J. A. Mikroyannidis, A. N. Kabanakis, S. S. Sharma and G. D. Sharma, *Adv. Funct. Mater.*, 2011, **21**, 746–755.
24 Y. Zhang, J. Zou, C.-C. Cheuh, H.-L. Yip and A. K.-Y. Jen, *Macromolecules*, 2012, **45**, 5427–5435.
25 B. C. Schroeder, R. S. Ashraf, S. Thomas, A. J. P. White, L. Biniek, C. B. Nielsen, W. Zhang, Z. Huang, P. S. Tuladhar, S. E. Watkins, T. D. Anthopoulos, J. R. Durrant and I. McCulloch, *Chem. Commun.*, 2012, **48**, 7699–7701.
26 A. Gadisa, M. Svensson, M. R. Andersson and O. Inganäs, *Appl. Phys. Lett.*, 2004, **84**, 1609.
27 M. F. Lo, T. W. Ng, T. Z. Liu, V. A. L. Roy, S. L. Lai, M. K. Fung, C. S. Lee and S. T. Lee, *Appl. Phys. Lett.*, 2010, **96**, 113303.
28 M. A. Loi, S. Toffanin, M. Muccini, M. Forster, U. Scherf and M. Scharber, *Adv. Funct. Mater.*, 2007, **17**, 2111–2116.
29 C. Deibel, T. Strobel and V. Dyakonov, *Adv. Mater.*, 2010, **22**, 4097–4111.
30 K. Vandewal, A. Gadisa, W. D. Oosterbaan, S. Bertho, F. Banishoeib, I. Van Severen, L. Lutsen, T. J. Cleij, D. Vanderzande and J. V. Manca, *Adv. Funct. Mater.*, 2008, **18**, 2064–2070.
31 B. Yang, J. Cox, Y. Yuan, F. Guo and J. Huang, *Appl. Phys. Lett.*, 2011, **99**, 133302.
32 M. Hallermann, I. Kriegel, E. Da Como, J. M. Berger, E. von Hauff and J. Feldmann, *Adv. Funct. Mater.*, 2009, **19**, 3662–3668.